INFLUENCE OF SECONDARY FLOW PHENOMENA ON BOUNDARY LAYER THICKNESS AND WALL HEAT FLUX IN SCALLOPED RADIAL TURBINES

C. Rakut - D. Diefenthal - M. Wirsum

Institute for Power Plant Technology, Steam and Gas Turbines
RWTH Aachen University, Templergraben 55
D-52056 Aachen, Germany
office@ikdg.rwth-aachen.de

ABSTRACT

This paper deals with investigations of the boundary layer and the influencing flow phenomena in radial turbine wheels. Therefore the interrelationship between secondary flow phenomena, boundary layer thickness, thermodynamic state at the edge of the boundary layer and the wall heat flux is investigated. The results based on experimental and numerical heat transfer investigations of a scalloped turbocharger turbine wheel for commercial application. The investigations are performed and calculated for steady state operating points with a total turbine inlet temperature of 600°C. The numerical investigations aim to model the flow field and the heat transfer between the fluid and solid state and provide the basis for the following considerations. For the determination of the boundary layer thickness six criteria based on the flow velocity and the velocity gradient were defined. The evaluation of the thermodynamic state at the boundary layer edge show a relation between this thermodynamic state and the wall heat flux and enable a better understanding of the characteristic of the wall heat flux distribution and the specific conditions if there is a local heat input to or heat output from the radial turbine wheel.

KEYWORDS

Radial Turbine, Boundary Layer, Secondary Flow Phenomena, Conjugate Heat Transfer

NOMENCLATURE

c	Flow velocity
ṁ	Mass flow rate
Ma	Mach number
p	Pressure
q̇	Heat flux
R	Specific gas constant
T	Temperature
y^+	Dimensionless wall distance
u	Circumferential velocity
α	Heat transfer coefficient
κ	Isentropic exponent

Subscripts

0, ref	Reference
C	Compressor
h	Housing
I	Inlet
MP	Measuring point turbine wheel
O	Outlet
T	Turbine
tot	Total

Abbreviations

MP	Measuring point turbine wheel
CFD	Computational Fluid Dynamics
CHT	Conjugate Heat Transfer
Exp.	Experimental
FEA	Finite Element Analysis
IKDG	Institut for Power Plant Technology, Steam and Gas Turbines

INTRODUCTION

In recent years there has been a trend towards higher inlet temperatures of turbocharger turbines. Already in 2006 gas temperatures up to 1050°C were reached in gasoline fired engines (Dornhöfer et al., 2006). Because of the higher turbine inlet temperatures, thermomechanical fatigue issues gained importance. In the last years a number of studies related to thermomechanical fatigue in turbochargers were published. Heuer et al. (2006) performed transient fluid/solid heat transfer calculations for a turbine wheel and validated the results by means of steady state measurements. The authors showed that the centrifugal loads are dominant with respect to the thermomechanical stresses in the turbine wheel, the thermal loads were shown to be significant as well, however.

Oberste-Brandenburg et al. (2012) developed a simplified model for the calculation of the transient temperature field in a turbine housing of a turbocharger. In this approach the time consuming CFD simulations are replaced by a simple 1D model. This approach shows a good agreement with CFD calculations when comparing averaged heat transfer coefficients. However, the predicted plastifications show significant differences between the simplified model and the detailed model.

An alternative approach was presented by Ahdad et al. (2010). The authors use a semi-empirical model to calculate the thermal stresses in the turbine housing. The model was developed and validated by means of FEA calculations. Due to the empirical correlations used in this model, it has to be calibrated for different turbine housing geometries.

In the last years experimental and numerical investigations regarding the temperature gradients, the thermal loads and the heat transfer in turbochargers were conducted at the IKDG. Examples are Diefenthal et al. (2014, 2015, 2016) and Tadesse et al. (2015). In Rakut et al. (2016) the analysis of the heat transfer in a radial turbine wheel is presented and the prediction of the heat transfer coefficients with an empirical method is described.

The focus of this paper is the determination of the boundary layer thickness in radial turbine wheels with respect to the heat transfer between fluid and solid. A better understanding of the interrelationship between secondary flow phenomena, the boundary layer thickness, the thermodynamic state at the edge of the boundary layer and the wall heat flux will help to improve the methods to predict the heat transfer coefficients. In order to investigate this interrelationship, CHT calculations were conducted and validated by experimental data from a test rig for steady state operating points.

EXPERIMENTAL SETUP

In the present work a scalloped turbine wheel of a commercial vehicle turbocharger with a wheel diameter of about 90 mm is investigated. The turbocharger has a double-flow volute. In order to analyze the steady state temperature field in the turbine wheel and to validate the CHT calculations an existing test rig was modified to measure material temperatures on the turbine wheel during operation.

The schematic of the test rig is shown on the left side in Fig. 1. The air used in the combustion chamber is supplied by a turbo compressor. The hot gas mass flow with a turbine inlet temperature of 600°C is provided by an oil-fired combustion chamber. The mass flow rate is measured by an orifice plate. In upstream direction of the turbine inlet a flow conditioner is used to provide a similar flow profile in every operating point. The compressor of the turbocharger is operated in a separated closed loop and can be throttled to adjust the operating point. The mass flow of the compressor is measured by an orifice plate as well. In order to achieve a constant compressor inlet temperature the air mass flow is cooled by a water cooler.

To determine the thermodynamic operating conditions of the turbocharger, the pressure and the temperature are measured at the inlet and the outlet of the compressor and the turbine. In all four measurement planes several type K thermocouples are applied along the circumference. The diameters of the sensors of the thermocouples are 1.5 mm on the compressor side and 0.5 mm on the turbine side. Additionally the rotational speed is recorded.

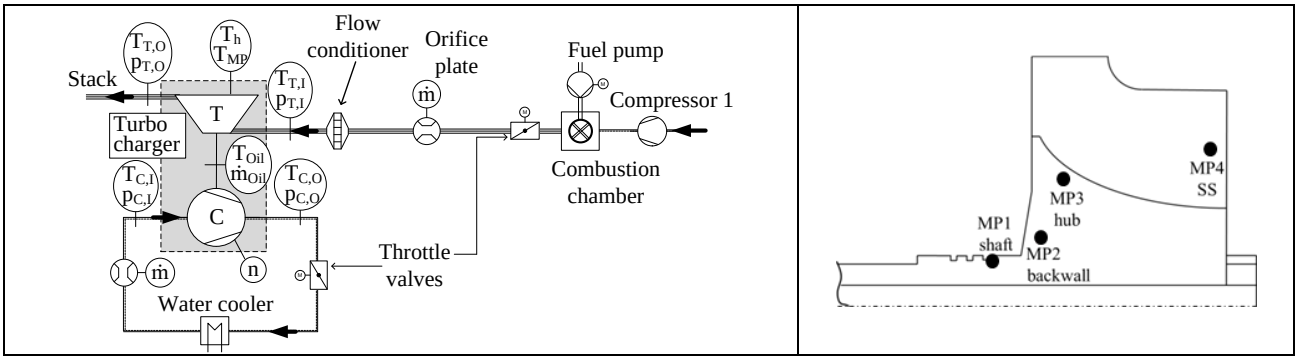

Fig. 1 Scheme of the test rig for steady state operating points (left) and Position of the thermocouples at the turbine wheel (right)

To measure the temperatures on the turbine wheel during the operation four type K thermocouples are mounted in the turbine wheel. The modification of the turbine wheel was made similar to the system described by Heuer et al. (2005, 2006). The individual positions of the thermocouples are shown at the right side in Fig. 1. The thermocouples in the turbine wheel are connected to a transmitter, which is located at the shaft end near the compressor inlet. The transmission of amplified signals from the rotating to the stationary system is done by using a telemetry system. Additional type K thermocouples are attached on the outer surface of the turbine housing to record the temperature distribution. A more detailed description of the test rig and the measurement setup for transient operation of a turbocharger between different temperature levels is given by Tadesse et al. (2015).

A turbine operation map with six defined rotor speeds and five or six steady state operating points at each rotor speed was measured at a constant turbine inlet temperature of 873 K. The boundary conditions for the numerical investigations were derived from the recorded data at the inlet and outlet measurement planes of the turbocharger.

NUMERICAL MODEL

The model for the CHT calculations comprises the turbine housing, the turbine wheel and the inlet and outlet pipes. Due to the high computational effort the bearing housing and the compressor are not included. He and Oldfield (2011) showed that the timescale of convection in the fluid and conduction in the solid state differs about a factor of 10^4. In other words, temperature changes in the solid state run much slower than unsteady effects in the fluid. For the investigations the temperature field in the solid state, the wall temperature and the mean flow conditions are of interest. Thus unsteady effects in the flow play a minor role regarding the investigated steady state heat transfer and the turbine wheel is modelled as a 40 degree segment by using periodical boundary conditions. The transformation from the non-rotating to the rotating system is performed by peripheral averaging (stage interface). The model is depicted in Fig. 2. As boundary conditions for the fluid state, the total pressure and the total temperature are assumed to be constant at the inlet. At the outlet the radial pressure equilibrium is calculated based on the measured wall pressure. As can be

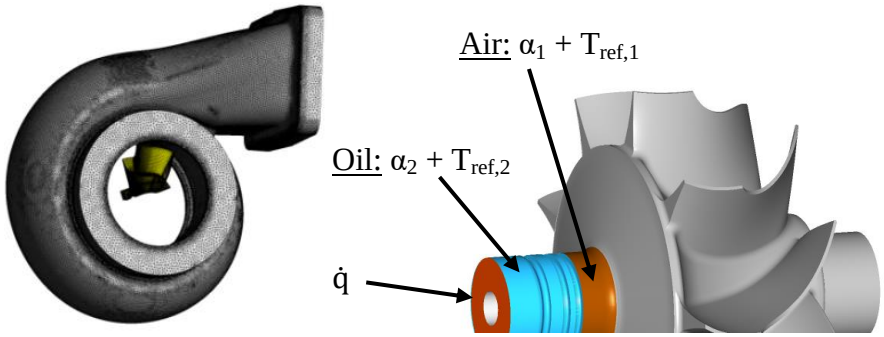

Fig. 2 Numerical model without inlet and outlet pipes

seen in Fig. 2 three areas are defined on the surfaces of the shaft, each with boundary conditions that describe the heat fluxes to the oil and through the shaft. On the surfaces of the shaft that are surrounded by oil and air respectively, two constant heat transfer coefficients and reference temperatures are used. At the cut of the shaft a constant specific heat flux is defined. This heat flux and the heat transfer coefficients are iteratively varied until the root mean square deviation between measured and calculated temperatures at measuring points 1 and 2 is minimal. This calibration is performed for all investigated operating points. The heat shield is assumed to be adiabatic.

The mesh of the whole turbine model consists of approximately 6.2 million nodes. 3.7 million nodes are located in the fluid and 2.5 million nodes discretize the solid body. In the fluid boundary layer a dimensionless wall distance lower than y+ = 1.0 is implemented. The mesh in the boundary layer of the solid body is highly resolved as well. A mesh study with five different mesh densities between 2.5 million and 7.6 million nodes has been conducted to ensure that the results are unaffected by the mesh. To model the turbulence in the thermal sublayer, the low Reynolds kω-SST turbulence model (Menter, 1993) is used. All calculations are conducted with ANSYS CFX 15.0. In Tab. 1 the comparison of measured and calculated results for five operating points are shown. The reference u_0 represent the highest circumferential velocity of the turbine and the reference $\dot{m}_{T,0}$ the highest turbine mass flow of the turbocharger. A more detailed description and validation of the CHT calculations can be found in Diefenthal et al. (2014, 2015).

	u/u_0 [-]	$\dot{m}_T/\dot{m}_{T,0}$ [-]	MP 1 [K]	MP 2 [K]	MP 3 [K]	MP 4 [K]	$T_{T,O}$ [K]
Exp.	0.61	0.426	564.2	761.9	787.3	805.9	789.1
CHT		0.426	591.0	758.9	788.0	802.5	788.5
Exp.	0.74	0.595	575.2	756.7	779.8	786.7	754.2
CHT		0.593	590.1	753.6	778.4	784.2	754.6
Exp.	0.85	0.704	555.2	748.6	774.9	775.9	732.4
CHT		0.700	555.7	747.8	776.3	776.1	733.1
Exp.	0.935	0.872	566.1	751.2	775.8	765.4	708.6
CHT		0.863	563.6	754.3	782.0	773.6	710.4
Exp.	1.0	0.953	564.6	755.1	779.2	767.4	695.7
CHT		0.945	564.1	757.2	784.7	772.3	697.4

Tab. 1 Comparison of measured and calculated turbine mass flow, solid temperatures in the turbine wheel and the fluid temperature at turbine outlet for five operating points

The analysis of the heat transfer characteristics and the derivation of the empirical model to describe the heat transfer between the fluid and the solid are based exclusively on the validated results of the CHT calculations.

BOUNDARY LAYER CONSIDERATIONS

Aero-thermodynamic in the Boundary Layer

In the boundary layer the undisturbed main velocity is decelerated and at the wall adhesion condition exists. The total temperature of the flow represents the superposition of the static temperature and the velocity. In equation (1) the relation between the total and the static temperature is given as a function of the Mach number.

$$\frac{T_{tot}}{T} = 1 + \frac{\kappa - 1}{2} \cdot \frac{c^2}{\kappa R T} = 1 + \frac{\kappa - 1}{2} \cdot Ma^2 \tag{1}$$

Through the deceleration of the flow the static temperature rises and at the wall the static temperature is equal to the total temperature. This is shown in Fig. 3 for normalized velocity and temperatures. In the ideal case without losses and for small velocities the total temperature is constant. In the considered case the overshooting and the decreasing of the total temperature near the wall are caused by two mechanisms. The losses in the boundary layer through the deceleration causes a rising static temperature level nearly in the whole boundary layer but mainly in the area of the high velocities. This leads to the overshooting. In the laminar sublayer the conductive heat transport dominates and heat is transported out of this sublayer and decreases the static temperature level near the Wall. This causes the decreased total temperature.

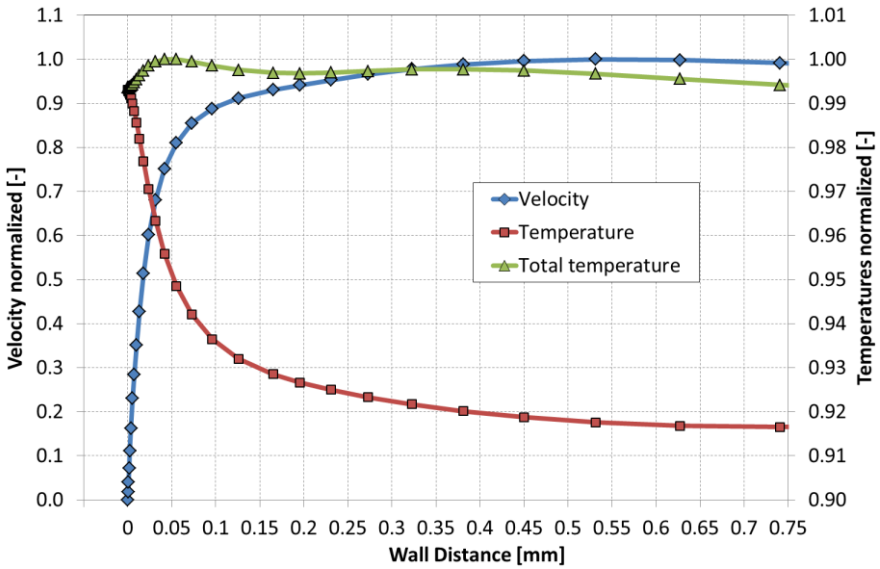

Fig. 3 Profiles for velocity, static temperature and total temperature in the boundary layer

Boundary Layer Thickness

To determine the boundary layer thickness of the blade flow the velocity profile normal to the blade surface has to be obtained. Therefore a normal vector was built in each surface node of the numerical model and the velocity data were readout at 30 sampling points. For the distribution of the sampling points along the vector a rising space between adjacent points was chosen similar to the boundary mesh resolution of the numerical model. For the evaluation of the boundary layer thickness six criteria were defined. These criteria are shown in Fig. 4 in schematic diagrams. The first main criterion is A) the maximum velocity whereby the boundary layer thickness is defined to 99.5 % of the undisturbed blade channel velocity. For the undisturbed blade channel velocity, the maximum velocity along the normal vector in the investigated distance to the wall is assumed. For this case the distance is chosen to 1.0 mm which is nearly twice of the found boundary layer thickness. The second main criterion is B) a threshold value for the velocity gradient normal to the surface which has to be defined. This criterion is useful if the velocity is rising with a small gradient which is caused through disturbance of the secondary flow phenomena. The threshold value is chosen to 0.1 (m/s)/µm. Criteria A) and B) are used for classical boundary layer velocity profiles and the criterion with the lowest distance to the wall defined the boundary layer thickness.

The four following criteria C) to F) are needed if the velocity profiles do not match with a classical boundary layer velocity profile. This for example may be caused by an overlapping vortex which can lead to a staged velocity profile (C, D). A staged velocity profile means that there is no local maximum of the velocity and that the velocity gradient in the stage is positive. The criterion C) “first local velocity gradient minimum” is used if a stage is localized at high velocities near the potential edge of the boundary. The contribution of the rising velocity over the defined threshold to the temperature gradient in the boundary layer is negligible. Furthermore the

temperature gradient in the region of the minimum velocity gradient and thus the heat transport in the fluid decreases strongly. In this case the threshold for criterion C) is set to 75 % of the maximum velocity. If the velocity stage is located under 75 % of the maximum velocity or near the wall in the region of low velocities criterion D) is used. The velocity gradient over the stage is typically small but greater than zero and thus the temperature gradient also. The high velocity change after the stage dominates the temperature gradient in the boundary layer. The threshold value of the velocity gradient for criterion D) is also chosen to 0.1 (m/s)/µm. Criterion E) is used if the velocity increases slightly without forming a stage or a maximum. In this case the boundary layer thickness is defined to the location with the "second local minimum of the velocity gradient". In cases where the velocity gradient is constant after a large velocity increase and higher than the threshold of 0.1 (m/s)/µm for criterion B) the criterion F) is used. Here a threshold value of -0.005 (m/s)/µm² for the second derivative of the velocity is set. The slightly velocity increase after the found boundary layer thickness has an insignificant influence to the temperature gradient and the heat flux in the boundary layer.

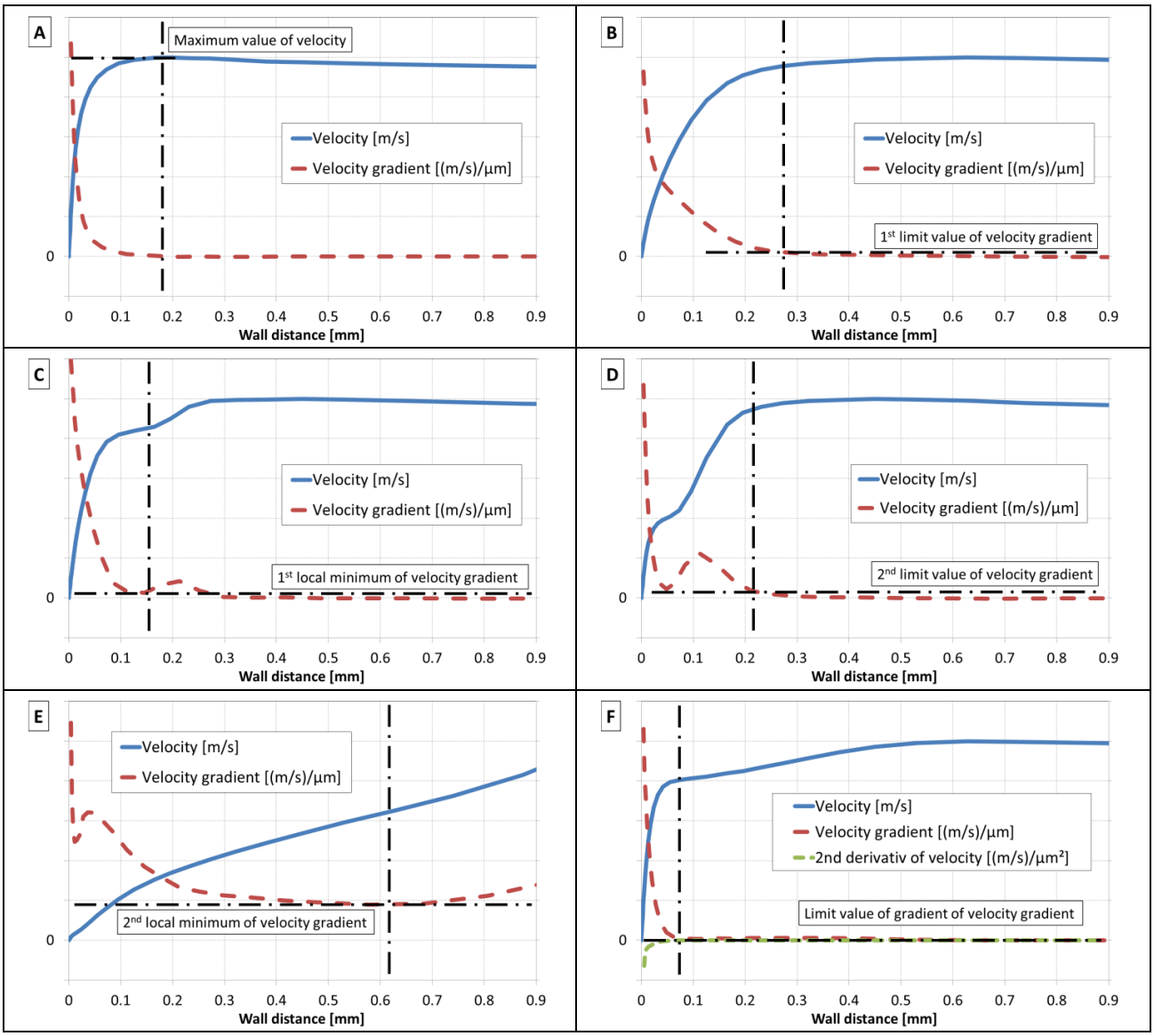

Fig. 4 Defined criteria to evaluate the boundary layer thickness

For four operating points the boundary layer thickness at suction side is shown in Fig. 5. Beginning from the inlet the boundary layer thickness increases continuously along the flow path for all operating points and shows an abrupt decrease near the trailing edge in a global point of

view. This sudden change represents in all cases the beginning of the flow separation zone, where a new boundary layer starts with a small boundary layer thickness. For all cases there are local areas with a higher boundary layer thickness compared to the surrounding areas. One of these areas is located at the same region near the hub for all operating points. For the lowest operating point (A) there is also a single area located near the blade back and the boundary layer thickness increases especially near the blade tip. A band of higher boundary layer thickness is shown for the cases (B) to (D) which starts near the turbine wheel inlet and ends near the sudden change. The radial position of these band decreases with the rising circumferential velocity. For these three cases there is also a band of low boundary layer thickness starting at the corner leading edge / blade tip and extends along the blade tip to the beginning of the flow separation area. This band results from the vortex induced at the corner leading edge / blade tip. The development and growth of this vortex is described in detail in Rakut et al. (2016).

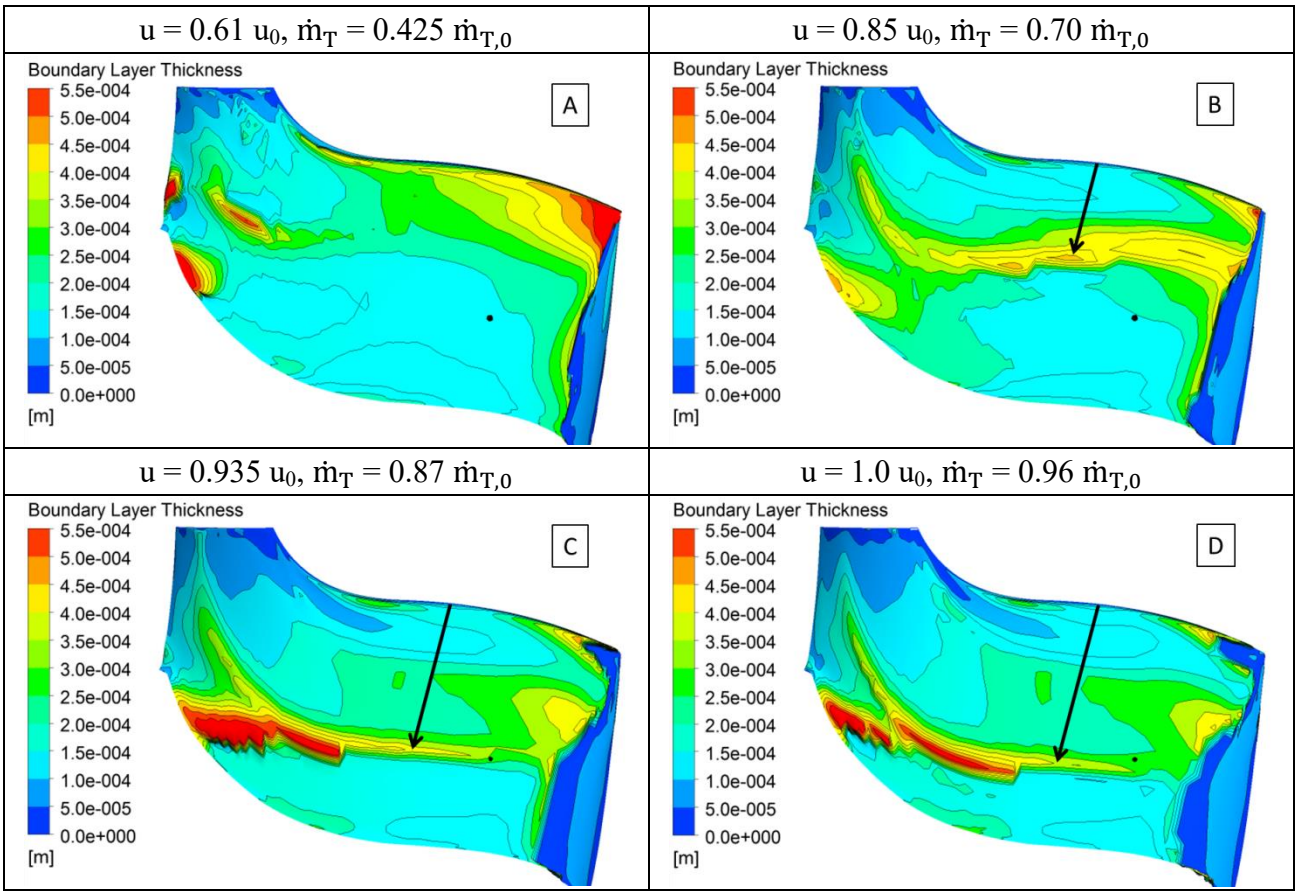

Fig. 5 Boundary layer thickness at suction side for four operating points, $T_{tot,TI}$ = 873 K

Secondary Flow Phenomena

In Fig. 6 secondary flow phenomena for two operating points are shown. In the left column (A, C) an overview of the suction side is depicted and in the right column (B, D) the turbine wheel inlet is shown. The flow vectors illustrate the flow in the boundary layer in a wall distance of 0.1 mm. The direction of the vectors show that the areas with a higher boundary layer results from the clash and redirection of different sub flows. In comparison of the left column it can be seen that the flow in the boundary layer for high operating points (C) has for flow path length greater than 50% a strong axial orientation whereas for lower operating points (A) a more centrifugal orientation dominates. This corresponds with the band of higher boundary layer thickness (Fig. 5, B-D) whose radial position differs with the operating point. Both pictures show that the area with higher

boundary layer thickness near the hub is caused by several flows starting in the axial gap and a cross flow from pressure side. The occurrence of this area is independent from the operating point.

The area near the back of the blade with the higher boundary layer thickness for the lower operating point, results from two opposed oriented flows which start in the axial gap. This is illustrated in Fig. 6 (B). Both figures in the right column show the different flow orientation in the boundary layer at the turbine wheel inlet. For lower operating points (B) the flow in the boundary layer has a mainly axial orientation and a high flow part enters the blade channel from the axial gap. The boundary flow at the turbine wheel inlet has for higher operating points (D) the expected centripetal orientation

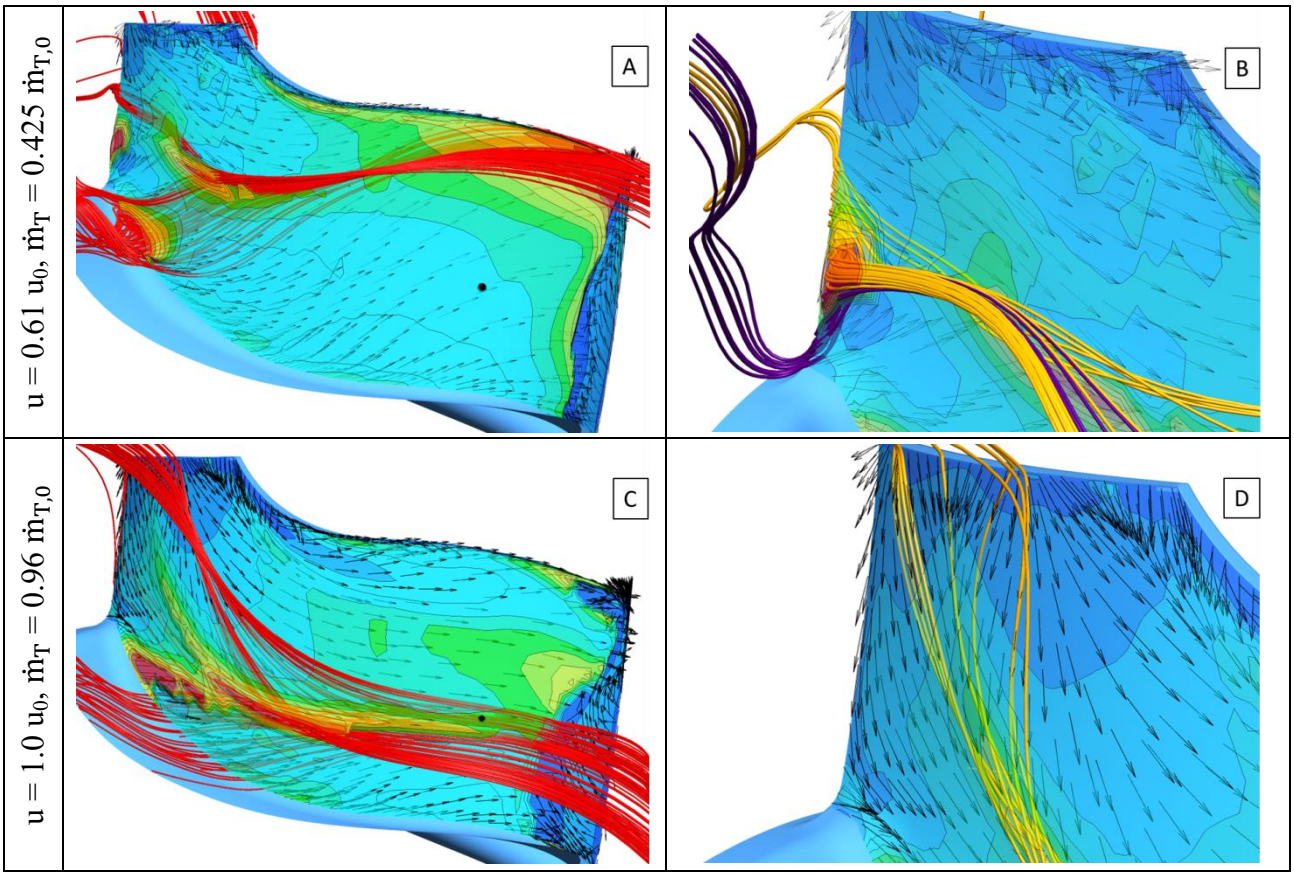

Fig. 6 Secondary flow phenomena at suction side for two operating points, $T_{tot,TI}$ = 873 K

Aero-Thermodynamic State at the Edge of the Boundary Layer

For a high operating point the aero-thermodynamic state at the edge of the boundary layer is shown in Fig. 7. Picture A) shows the boundary layer thickness, picture B) the relative Mach number, picture C) the relative total temperature and picture D) the static temperature. Both temperatures (C, D) and the relative Mach number (B) are linked by eq. (1). The profile of the aero-thermodynamic parameters with high gradients at the leading edge result through the superposition of low boundary flows from the volute and the circumferential velocity. This phenomenon is discussed in detail in Rakut et al. (2016). For the relative total temperature (C) the strong differences in the profile at the leading edge are maintained up to 40 % of the flow path. The strong gradient of the relative total temperature (C) for a constant radius near the axial gap side coincide with the band of the higher boundary layer thickness (highlighted area 1). Fig. 6 (D) shows that the band of higher boundary layer thickness in this area results from the interaction of the centripetal stream lines from the mid of the leading edge and the more axial oriented stream lines starting at the corner leading edge / axial gap. The relative total temperature in Fig. 7 (C) is, as expected, for flow path length over 40 % nearly constant for a constant blade height and proportional to the

circumferential velocity. Near the trailing edge a discontinuity occurs and following the relative total temperature decreases for a constant radius. The discontinuity corresponds with the above-mentioned beginning of the new boundary layer in the flow separation zone.

The relative Mach number (B) at the edge of the boundary layer continuously increases beginning from the inlet and shows a decrease near the trailing edge from a global point of view. The static temperature (D) shows an opposite behavior with a decrease beginning from the leading edge and an increase near the trailing edge. This behavior of the relative Mach number (B) and the static temperature (D) in the area of constant relative total temperature (C) comply with eq. (1). For both thermodynamic parameters the sudden change also corresponds with the beginning of the new boundary layer in the flow separation zone.

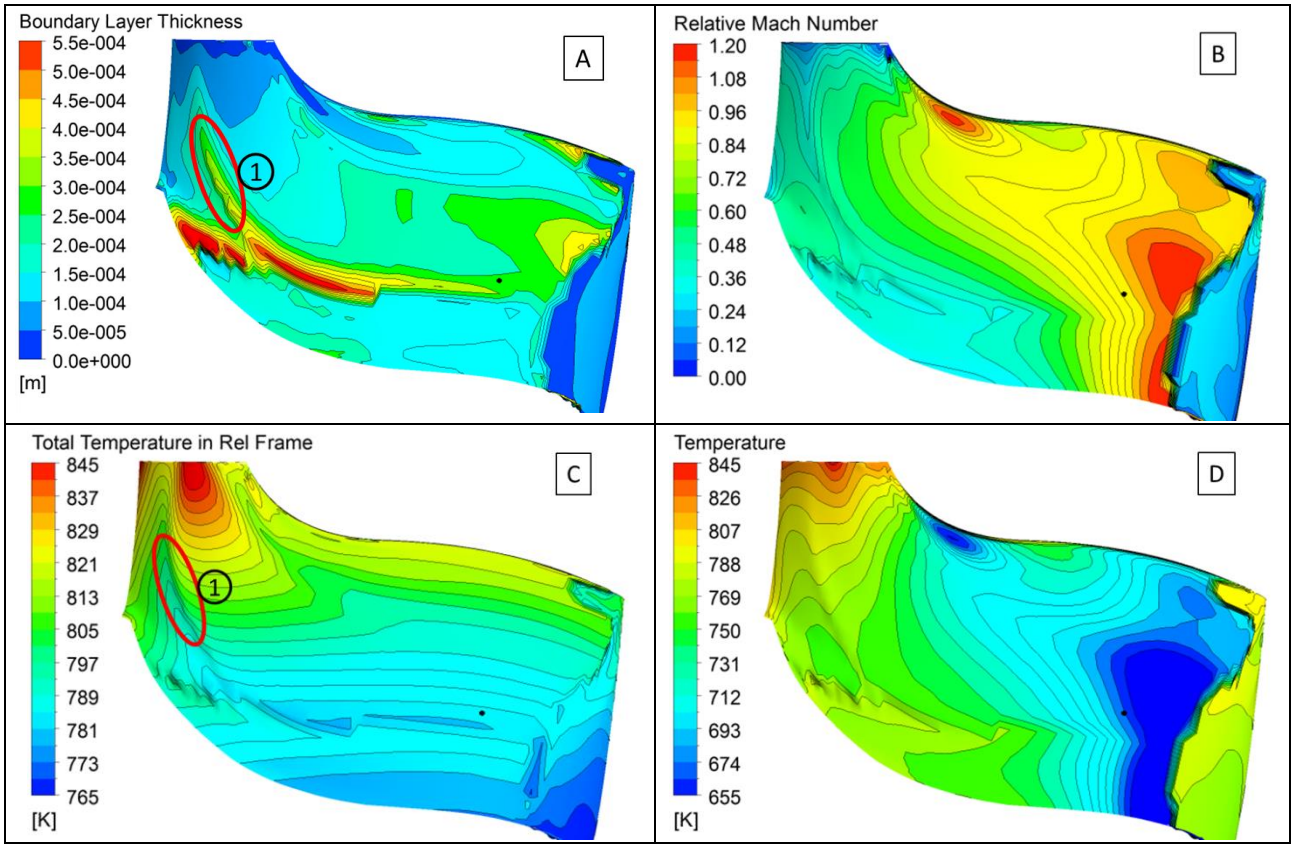

Fig. 7 Aero-thermodynamic state at the edge of the boundary layer $u = 1.0\ u_0$, $T_{tot,TI} = 873$ K, $\dot{m}_T = 0.96\ \dot{m}_{T,0}$

Wall Heat Flux and Boundary Layer Thickness

In Fig. 8 the comparison of the wall heat flux and the boundary layer for a low (A, B) and a high (C, D) operating point is shown. In a general point of view the boundary layer thickness and the wall heat flux develops in an opposite manner. A low boundary layer thickness corresponds with a high positive heat flux from the flow to the blade surface and a high thickness with a high negative heat flux from the surface to the fluid. In the flow separation zone, the low boundary layer thickness corresponds also with a high positive heat flux from the fluid to the blade surface. For the lower operating point (A, B) in the two areas with a high boundary layer thickness near the axial gap and the hub the wall heat flux decreases compared to the surrounding area. For the higher operating point (C, D) the beginning of the band of the higher boundary layer thickness corresponds with the strong wall heat flux gradient between the heated and cooled area.

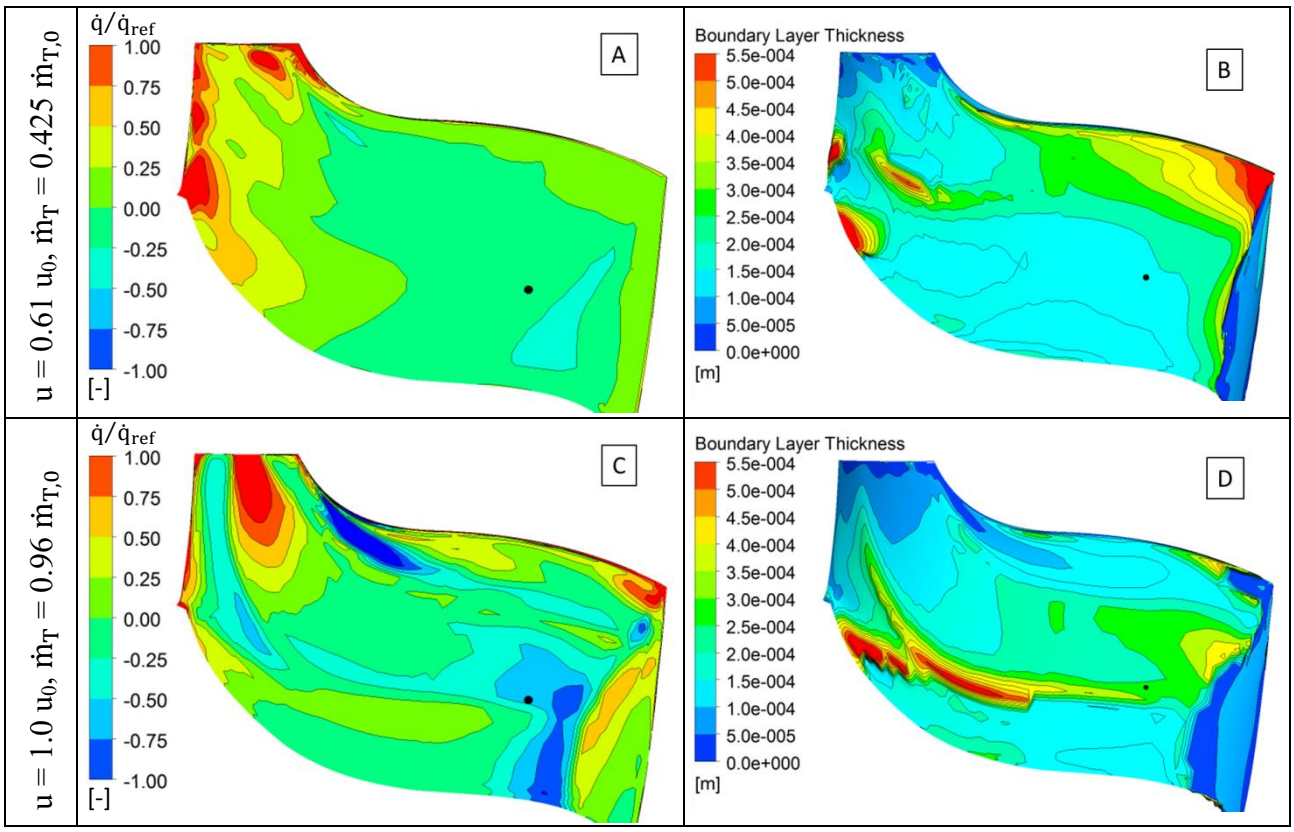

Fig. 8 Comparison of Wall heat flux and boundary layer thickness at suction side for two operating points, $T_{tot,TI}$ = 873 K

CONCLUSIONS

In the presented paper six criteria for the determination of the boundary layer thickness for different boundary layer velocity profiles were defined and the boundary layer thickness at the suction side of a radial turbine wheel was determined using these criteria. Several secondary flow phenomena were identified which influences the characteristic of the boundary layer thickness. Thus it could be shown that the local increases of the boundary layer thickness are attributable to the convergence of different oriented flows in the boundary layer. Through the convergence of flows starting at the leading edge, the axial gap and cross flows from the pressure side, a long band of a local increase of the boundary layer thickness is caused. The position of this band is influenced through the operating point. The flow separation zone at the trailing edge was identified for all operating points. Here a new boundary layer with a low boundary layer thickness starts. The aero-thermodynamic state at the edge of the boundary layer was analyzed and the wall heat flux distribution was compared with the characteristic of the boundary layer thickness.

ACKNOWLEDGEMENTS

The authors would like to thank the research association Forschungsvereinigung Verbrennungskraftmaschinen e. V. and the Association Industrial Research (AIF) for the financial support of this research project. The authors would like to gratefully acknowledge BorgWarner Turbo Systems whose support was essential for the presented investigations. Furthermore the authors gratefully acknowledge the computing time granted by the JARA-HPC Vergabegremium and provided on the JARA-HPC partition's part of the RWTH Bull Cluster in Aachen / the supercomputer JUQUEEN at Forschungszentrum Jülich.

REFERENCES

Ahdad, F., Kannusamy, R., Damodharan, B., (2010). *Analytical Approach of TMF Prediction for Complex Loading.* ASME Turbo Expo GT2010-23440, Glasgow, UK

Diefenthal, M., Tadesse, H., Rakut, C., Wirsum, M., (2014) *Experimental and numerical investigation of temperature fields in a radial turbine wheel*. 15th International Symposium on Transport Phenomena and Dynamics of Rotating Machinery, ISROMAC-15, Honolulu, USA

Diefenthal, M., Rakut, C., Tadesse, H., Wirsum, M., Heuer, T., (2015). *Temperature Gradients in a Radial Turbine in Steady State and Transient Operation*. International gas turbine conference, Tokyo, Japan

Diefenthal, M., Hopfinger, M., Rakut, C., Wirsum, M., Heuer, T., (2016). *Thermomechanical analysis of transient temperatures in a radial turbine wheel*. ASME Turbo Expo GT2016-56328, Seoul, South Korea

Dornhöfer, R., Hatz, W., Eiser, A., Böhme, J., Adam, S., Unselt, F., Cerulla, S., Zimmer, M., Friedemann, K., Uhl, W. (2006). *Der neue R4 2,0l 4V TFSI-Motor im Audi A3.* 11. Aufladetechnische Konferenz, Dresden, Germany

He, L., Oldfield, M. L. G., (2011). *Unsteady Conjugate Heat Transfer Modeling*. ASME Journal of Turbomachinery, 133, No. 3, July

Heuer, T., Engels, B., Wollscheid, P., (2005). *Thermomechanical analysis of a turbocharger based on conjugate heat transfer*. ASME Turbo Expo, GT2005-68059, Reno-Tahoe, USA

Heuer, T., Engels, B., Klein, A., Heger, H., (2006). *Numerical and experimental analysis of the thermo-mechanical load on turbine wheels of turbochargers*. ASME Turbo Expo GT2006-90526, Barcelona, Spain

Menter, F.R., (1993). *Zonal two equation k ω turbulence models for aerodynamic Flows*. AIAA paper 93-2906

Oberste-Brandenburg, C., Shoghi, K., Gugau, M., Kruse, F., (2012). *On the influence of thermal boundary conditions on the Thermo-Mechanical Analysis of turbine housing of a turbocharger*. Proceedings of 10th International Conference on Turbochargers and Turbocharging, pp 83-95, London, UK

Rakut, C., Diefenthal, M., Wirsum, M., Heuer, T., (2016). *Analysis of heat transfer in a radial turbine wheel of turbochargers and prediction of heat transfer coefficients with an empirical method.* ASME Turbo Expo GT2016-57687, Seoul, South Korea

Tadesse, T., Rakut, C., Diefenthal, M., Wirsum, M., Heuer, T., (2015). *Experimental investigation of steady state and transient heat transfer in a radial turbine wheel of a turbocharger*. ASME Turbo Expo GT2015-43165, Montreal, Canada